EUROPEAN ORGANIZATION FOR NUCLEAR RESEARCH

CERN-EP/89-38
7 March 1989

REAL-TO-IMAGINARY RATIO OF THE $\bar{p}p$ FORWARD ELASTIC SCATTERING AMPLITUDE AT 550, 757, AND 1077 MeV/c

P. Schiavon[1], R. Birsa[1], K. Bos[2], F. Bradamante[1], A.S. Clough[5], S. Dalla Torre-Colautti[1], J.R. Hall[3*], E. Heer[4], R. Hess[4], J.C. Kluyver[2], R.A. Kunne[2**], C. Lechanoine-Leluc[4], L. Linssen[2×], A. Martin[1], Y. Onel[4××], A. Penzo[1], D. Rapin[4], R.L. Shypit[5], F. Tessarotto[1] and A. Villari[1]

ABSTRACT

The ratio of the real to the imaginary part of the $\bar{p}p$ forward elastic scattering amplitude ϱ has been measured at 550, 757, and 1077 MeV/c at LEAR, using the Coulomb-nuclear interference method. The results obtained for ϱ and b, the nuclear slope, are $\varrho = 0.084 \pm 0.051$ and $b = 20.9 \pm 2.1$ $(GeV/c)^{-2}$ at 550 MeV/c, $\varrho = 0.102 \pm 0.041$ and $b = 18.0 \pm 0.5$ $(GeV/c)^{-2}$ at 757 MeV/c, and $\varrho = 0.059 \pm 0.033$ and $b = 15.2 \pm 0.3 (GeV/c)^{-2}$ at 1077 MeV/c.

(Submitted to Nuclear Physics B)

---

1) INFN Trieste and University of Trieste, Italy.
2) NIKHEF-H, Amsterdam, The Netherlands.
3) Queen Mary College, London, UK.
4) DPNC, University of Geneva, Switzerland.
5) University of Surrey, Guildford, Surrey, UK.

Present addresses:
*) BNL, Upton NY, USA.
**) DPNC, University of Geneva, Switzerland.
×) CERN, Geneva, Switzerland.
××) University of Iowa, Iowa City, Ia, USA.

1. INTRODUCTION

We have measured ϱ, the ratio of the real to the imaginary part of the $\bar{p}p$ forward elastic scattering amplitude, at 550, 757, and 1077 MeV/c using the Coulomb–nuclear interference method. The measured values are in a momentum region where the available data are rather scattered (between 400 and 700 MeV/c) or non-existent (between about 700 and 1100 MeV/c) (see refs. [1] to [8]). The data have been collected at the Low-Energy Antiproton Ring (LEAR) at CERN in an experiment, carried out as part of the PS172 experimental programme [9], intended to measure asymmetry effects in $\bar{p}$ scattering off carbon and hydrogen [10, 11]. The small-angle scattering data have been used to extract ϱ along the same lines as a previous measurement already done by the Collaboration at 233 and 272 MeV/c [12]. We note that the experimental apparatus was optimized to the $\bar{p}C$ and $\bar{p}p$ asymmetry measurements. Preliminary results were shown in 1987 at the 4th LEAR Workshop on Physics at LEAR with Low-Energy Antiprotons [13].

2. APPARATUS AND TRIGGER

The data at 550 MeV/c and those at 757 and 1077 MeV/c have been collected, under slightly different experimental conditions, during two separate runs, the former in June 1984 and the latter in August 1986. Both experimental layouts have already been described in detail in refs. [10] and [11], respectively.

The apparatus (fig. 1) consisted of a liquid-hydrogen target (LHT), multiwire proportional chambers (MWPCs), and scintillation counters.

The antiproton beam had a first focus 20 m upstream of the target, where counter B0 and a carbon scatterer (5.2 g/cm^2) were located. The purpose of the carbon was to try to polarize the antiprotons by scattering. The antiprotons that scattered elastically at an angle θ_C were focused by the beam channel into a system of two targets—a LHT and a carbon target—where their polarization was analysed as described in ref. [11]. Data were taken at $\theta_C = 8°$ at 550, 757, and 1077 MeV/c, where the scattered beam intensity was $\approx$ 200 $\bar{p}$ per second (low-intensity condition) and $\theta_C = 5°$ at 1077 MeV/c, where the scattered beam intensity was $\approx$ 1000 $\bar{p}$ per second (high-intensity condition).

Counters B1 (70 mm diameter, 0.5 mm thick) and B2 (30 mm, 0.5 mm), close to the target, defined the incoming particle. The time of flight (TOF) between B0 and B1 rejected the pion contamination ($< 10^{-3}$), and the momentum resolution of the beam line was about $\pm 1\%$.

The LHT had a length of 9.5 cm and a diameter of 3 cm; the target Mylar windows on the beam line had a total thickness of 650 μm. Counters S1–S5 surrounded the LHT (apart from a circular hole of 60 mm in S1 and one of 100 mm in S5 on the beam line), providing time-to-digital converter (TDC) information to identify annihilation events from the target in the off-line analysis.

The nominal values of the momenta of the LEAR extracted $\bar{p}$ beam were 600.8, 800, and 1100 MeV/c; the average beam momentum at the centre of the LHT was 550, 757, and 1077 MeV/c, respectively.

In the 550 MeV/c run (fig. 1a), chambers PC1 and PC2 (1 mm wire spacing) were used to measure the track of the incoming $\bar{p}$, and PC3–PC5 (2 mm wire spacing) the scattered particles.

In the 757 and 1077 MeV/c runs (fig. 1b), three MWPCs (PC1–PC3, 1 mm wire spacing) were used to measure the incoming track, and four chambers (PC4–PC6 and PC8, 2 mm wire spacing) measured the scattered one. Counters B0, B1, and B2 were the same, as were S1–S5 around the LHT. Moreover, counter V (80 mm diameter, 2 m downstream from the LHT) was used to reject events with a particle in the beam direction.

At 550 MeV/c and 1077 MeV/c (low intensity), the trigger condition was the coincidence B = B0*B1*B2. At 757 and at 1077 MeV/c (high intensity), in order to reject straight track events,

the first-level trigger was B* $\bar{V}$, and a second-level rejection was performed by the fast micro-programmable processor ESOP in the same way as in the 233 and 272 MeV/c measurements. The processor used the wires hit in the last MWPC to compute the distance between all the possible combinations of horizontal and vertical coordinates from the centre of the beam distribution on that chamber; the event was accepted only if all the computed distances were larger than a minimum value (chosen on the basis of beam spot and required geometrical acceptance at small angles), or if one or both planes were empty.

To determine the angular dependence of the $\bar{V}$*ESOP rejection in the off-line analysis at 757 and 1077 MeV/c, data samples were collected with the trigger B only, at the same time recording the information from counter V and from ESOP.

At all momenta, about 15% of the data were taken with the target empty to allow the evaluation and subtraction of the background due to particles scattered off the Mylar windows and the cryostat walls.

Table 1 lists the relevant statistics at the three momenta.

3. ANALYSIS OF THE DATA

In the off-line analysis, one — and only one — reconstructed track was required for the incoming and the outgoing particle in each set of MWPCs. In the track definition we asked for one hit in each chamber — at most, one chamber excepted — to be aligned, and for the incoming track to cross a fiducial circle of 22 mm diameter at the centre of the LHT around the beam line. If the two tracks met within less than 16 mm, an interaction vertex was defined, and we required δ, the distance of the vertex position along the beam axis to the centre of the LHT, to be such that $|\delta| \leq a + b/\theta$, where θ is the scattering angle (rad), and a = 39 (mm), b = 2 (mm·rad) at 757 and 1077 MeV/c; this dependence on the scattering angle of the resolution in the vertex position has been measured at the three momenta, using the sample of the elastic scattering events on hydrogen.

Most annihilation events were identified using the TDC information of counters S1–S5, which covered about 90% of the total solid angle. The residual annihilations were estimated to be about 3% (see refs. [10] and [11]). The remaining events were assumed to be elastically scattered.

To determine the elastic scattering events on hydrogen, the angular distribution of the events from the Empty Target (ET), normalized to the same number of useful incident $\bar{p}$, has been subtracted from the Full Target (FT) one.

At 757 and 1077 MeV/c, for the data taken with the trigger B* $\bar{V}$*ESOP, the angular acceptance has been evaluated by comparing the small-angle distribution of events collected with the B trigger only, but recorded with the information from counter V and ESOP, with the angular distribution of the same sample of events in which the rejection due to counter V and ESOP has been taken into account. The ratio of the latter to the former of the two distributions has been fitted to a fourth-order polynomial in θ^2, which has been used to correct the data at small angles. The accuracy of the evaluation is good: the residual systematic errors are about 0.2% and do not affect the value of ϱ. In the analysis, we accepted events for which the trigger efficiency is $\geq$ 50% of its maximum value (corresponding to $\theta \geq 1.4°$). At large angles, and at all momenta, we used an angular range (up to about $\theta = 15°$) corresponding to a full (100%) geometrical acceptance of the apparatus.

For the 757 and 1077 MeV/c data, we evaluated the particle absorption in the apparatus, which was due in particular to the carbon target for the $\bar{p}$C experiment run simultaneously and to the counter box surrounding it (fig. 1b), both of which were located between PC5 and PC6. We performed a Monte Carlo simulation, which used as input the angular distributions for scattering and annihilation of antiprotons in carbon and scintillators resulting from our measurements, and which

took into account the reconstruction efficiency of our analysis program. The main uncertainty is the value of the $\bar{p}C$ total cross-section (700 mb at 757 MeV/c and 645 mb at 1077 MeV/c) [14]. The measured differential elastic cross-sections, corrected for small-angle trigger efficiency and absorption losses, are listed in tables 2 to 4, together with the correction factors used.

4. FIT AND RESULTS

The $\bar{p}p$ differential cross-section is expressed in a conventional form as a sum of three terms: the Coulomb (C), the nuclear (N), and the Coulomb–nuclear interference. Using the notation of ref. [12], we have

$$d\sigma/dt = d\sigma_C/dt + d\sigma_{CN}/dt + d\sigma_N/dt \ ,$$

where

$$d\sigma_C/dt = 4\pi(\alpha \hbar c/\beta p^2)^2 \, \pi/X_c^2 f_m(\theta) \, f(t_s)^2 \ ,$$

$$d\sigma_{CN}/dt = (\alpha/\beta t_s) \, \sigma_{tot} \, f(t_s) e^{-bt/2} [\varrho \cos\delta(t) - \sin\delta(t)] \ ,$$

$$d\sigma_N/dt = \sigma_{tot}^2/(4\hbar c\sqrt{\pi})^2 (1 + \varrho^2)(1 + \eta^2) e^{-bt} \ ,$$

$$f(t) = (1 + t/0.71)^{-4} \ ,$$

$$\delta(t) = -[\ln(9.5t) + 0.5772] \, \alpha/\beta \ ,$$

with

- t being the four-momentum transfer in units of $(GeV/c)^2$;
- α the fine-structure constant;
- β the velocity of the $\bar{p}$;
- p the lab. momentum of the incident $\bar{p}$;
- X_c^2 a constant of the theory;
- $f_m(\theta)$ the Molière distribution for the single, plural, and multiple Coulomb scattering;
- t_s the four-momentum transfer corrected with a 'screening' term, as in ref [15], to prevent the Coulomb–nuclear differential cross-section from going to infinity at the scattering angle $\theta = 0$;
- η the parameter determining the spin dependence, is defined near the forward direction as $\eta^2 = (|\phi_1 - \phi_3|^2 + 2|\phi_2|^2)/|\phi_1 + \phi_3|^2$, where ϕ are the helicity amplitudes;
- $f(t)$ the electromagnetic form factor of the proton;
- $\delta(t)$ the phase of the Coulomb amplitude [16].

The differential elastic cross-section is parametrized as a function of ϱ, the real-to-imaginary ratio; b, the slope of the nuclear term; σ_{tot}, the $\bar{p}p$ total cross-section; and η (ϱ and b are assumed to be constant over the t-range considered).

To compare the theoretical $\bar{p}p$ differential elastic cross-section with the measured one, the former has been folded with the experimental resolution of the detector by means of the same procedure as that used by us in the low-momentum measurements [12] and discussed in detail in ref. [17]. As the folding function, we take the measured angular probability of scattering from the empty target, corrected for the calculated contribution due to the scattering off the hydrogen when the LHT is filled. At 550 MeV/c, the average value of the ET scattering angle was 8.8 mrad; at 757 and 1077 MeV/c, 9.1 and 6 mrad, respectively, owing to the presence of the carbon scatterer between

the MWPCs after the LHT. The folded cross-section is then fitted to the experimental angular distribution of the elastic scattering events on hydrogen.

In the fit, the parameters ϱ, b, σ_{tot}, and η are strongly correlated. In our case, σ_{tot}, which is well measured in independent experiments, has been kept fixed, and an overall normalization factor has instead been left free to allow small (up to 5%) adjustments of the value of the total detection and reconstruction efficiency (75%, 89%, and 76% at 550, 757, and 1077 MeV/c, respectively), which is known to a few percent. A three-parameter fit is recommended in order not to constrain the fit too much; in fact the extended t-range allows a good determination of the value of the nuclear slope b, and either σ_{tot} or the normalization factor should be fitted together with ϱ. Moreover, η has been neglected, assuming spin independence.

The results of the fits are summarized in table 5. The quoted errors for ϱ and b are statistical only. The contribution, due to the uncertainty in σ_{tot}, to the error of ϱ is ± 0.015 (± 2.2 mb) at 550 MeV/c, ± 0.017 (± 2 mb) at 757 MeV/c, and 0.017 (± 1.8 mb) at 1077 MeV/c. The values of σ_{tot} at 550 and 757 MeV/c have been extrapolated from our lower momentum measurements [18, 19], and at 1077 MeV/c have been taken from the literature [20]. The error in ϱ due to the uncertainty in the absorption corrections (assuming $\pm 10\%$ in $\sigma_{\bar{p}C}$) is 0.016 at both 757 and 1077 MeV/c, and the contribution due to the small-angle trigger rejection efficiency is negligible. The resulting total errors in ϱ are ± 0.051 at 550 MeV/c, ± 0.041 at 757 MeV/c, and ± 0.033 at 1077 MeV/c. At 1077 MeV/c, the low-intensity data (trigger B) and the high-intensity data (trigger B* $\bar{V}$*ESOP) have been fitted separately, and the results are in good agreement ($\varrho = 0.058 \pm 0.059$ and $\varrho = 0.050 \pm 0.026$, respectively).

Figure 2 shows the measured differential cross-sections at 550, 757, and 1077 MeV/c, respectively. The superimposed curves are the theoretical folded differential elastic cross-sections calculated by assuming for the parameters the values of the best fit. The lines extend over the range of bins used in the fit.

We have tried to determine the value of η from the fit, but, as is clear from the expression assumed for $d\sigma_N/dt$, a correlation is expected between η and ϱ and σ_{tot}. Leaving η as a free parameter in a three- or four-parameter fit does not allow a stable solution. Assuming that for η we have fixed values from 0.3 to 0.1 at the different momenta, as suggested by some models (refs. [21] to [23]), we obtain an appreciable change in the value of ϱ as expected, and also in the other fitted parameters, so that the results of the fits do not improve in a significant enough way to allow definite conclusions. Typically at 550 MeV/c, for $\eta = 0.3$ we get $\varrho = 0.15 \pm 0.05$ with a $\chi^2/\nu = 2.1$.

5. CONCLUSIONS

Figure 3 presents a compilation of the results of the ϱ measurements below 1.2 GeV/c, made with different experimental techniques from 1975 onwards and before the availability of the LEAR antiproton beams [1–6, 24], together with the LEAR results [7, 8, 12].

The figure shows a considerable spread of the values; this can in part be explained by the fact that a unique procedure for extracting ϱ from the measured data does not exist, and there are many different assumptions—mainly in the parametrization of the $\bar{p}p$ differential cross-section—that determine large variations in ϱ, whilst a meaningful comparison certainly requires a unified treatment. The ϱ-values from this experiment are somewhat lower with respect to the previous measurements below 700 MeV/c and around 1100 MeV/c, and also with respect to previous fits using dispersion relations [3, 5], but they agree with a new dispersion relation analysis [25] that takes into account all the recent LEAR data on ϱ [7, 8, 12] on σ_{tot} [18, 19], and on the s-wave scattering-length value obtained from the antiprotonic atoms [26, 27].

Acknowledgements

We wish to thank the LEAR machine staff for providing us with high-quality antiproton beams, and for their collaboration in solving many of operating problems.

REFERENCES

[1] H. Kaseno et al., Phys. Lett. **61B** (1976) 203.
[2] P. Jenni et al., Nucl. Phys. **B129** (1977) 232.
[3] H. Iwasaki et al., Phys. Lett. **103B** (1981) 247.
[4] M. Cresti et al., Phys. Lett. **132B** (1983) 209.
[5] H. Iwasaki et al., Nucl. Phys. **A433** (1985) 580.
[6] V. Ashford et al., Phys. Rev. Lett. **54** (1985) 518.
[7] W. Brückner et al., Phys. Lett. **158B** (1985) 180.
[8] W. Brückner et al., Proc. 4th LEAR Workshop on Physics at LEAR with Low-Energy Antiprotons, eds. C. Amsler et al., Villars-sur-Ollon, 1987 (Harwood Academic Publ., London, 1988) p. 277.
[9] R. Birsa et al., CERN/PSCC/79-55, PSCC/I6 (1979).
[10] R. Birsa et al., Phys. Lett. **155B** (1985) 437.
[11] A. Martin et al., Nucl. Phys. **A487** (1988) 563.
[12] L. Linssen et al., Nucl. Phys. **A469** (1987) 726.
[13] R. Birsa et al., same proceedings as ref. [8], p. 309.
[14] K. Nakamura et al., Phys. Rev. Lett. **52** (1984) 731.
[15] H. Øverås, CERN 63-9 (1963), pp. 1-11.
[16] M.P. Locher, Nucl. Phys. **B2** (1967) 525.
[17] L. Linssen, Ph.D. thesis, University of Amsterdam (1986).
[18] A.S. Clough et al., Phys. Lett. **146B** (1984) 299.
[19] D.V. Bugg et al., Phys. Lett. **194B** (1987) 563.
[20] V. Flaminio et al., CERN-HERA 84-01 (1984).
[21] P.H. Timmers et al., Phys. Rev. **D29** (1984) 1928.
[22] J. Côté et al., Phys. Rev. Lett. **48** (1982) 1319.
[23] M. Lacombe et al., Phys. Lett. **124B** (1983) 443.
[24] P. Jenni et al., Nucl. Phys. **B94** (1975) 1.
[25] P. Kroll and W. Schweiger, Wuppertal internal report WU B 88-27 (1988), and private communication.
[26] S. Ahmad et al., same Proceedings as ref. [8] , p. 717.
[27] L. M. Simons, ibid., p. 703.

Table 1

Statistics of the data collected at the three momenta. 'Events on DSTs' means the number of full target events after the pattern recognition filter, and 'elastic events' means the number of events left in the indicated t-range after all the applied cuts (vertex position, absorption contamination, etc.) and after subtraction of the empty-target events.

Momentum (MeV/c)	550	757	1077	
Useful beam	3.8	7.6	13.9	$\times 10^6$
Events on DSTs	1.4	1.5	4.2	$\times 10^6$
Elastic events	27.0	75.6	138.8	$\times 10^3$
Range in $-t$ (GeV/c)^2	0.30–19.6	0.26–43.3	0.48–81.6	$\times 10^{-3}$
Trigger	B	B* $\bar{V}$*ESOP	Both	

Table 2

The $\bar{p}p$ differential elastic cross-sections at 550 MeV/c. The quoted errors are statistical only.

θ^2 (rad^2)	$-t$ (GeV/c)^2	$d\sigma_m/dt$ [mb/(GeV/c)^2]	
0.0013	0.00039	14591.	± 280.
0.0019	0.00057	6486.	187.
0.0025	0.00076	3944.	146.
0.0031	0.00094	2660.	120.
0.0037	0.00112	2431.	114.
0.0045	0.00136	1950.	134.
0.0055	0.00166	1842.	130.
0.0065	0.00196	1464.	118.
0.0075	0.00226	1373.	111.
0.0085	0.00256	1391.	110.
0.0095	0.00286	1407.	104.
0.0105	0.00316	1288.	100.
0.0115	0.00346	1128.	99.
0.0125	0.00376	1454.	98.
0.0135	0.00406	1171.	100.
0.0145	0.00436	1226.	95.
0.0155	0.00466	1296.	95.
0.0165	0.00496	1313.	94.
0.0175	0.00526	1222.	86.
0.0185	0.00555	1252.	90.
0.0195	0.00585	1235.	96.
0.0205	0.00615	1188.	93.
0.0215	0.00645	1128.	95.
0.0225	0.00674	1061.	91.
0.0235	0.00704	1124.	87.
0.0245	0.00734	1086.	83.
0.0255	0.00763	1059.	80.
0.0265	0.00793	1144.	85.
0.0275	0.00822	1320.	84.
0.0285	0.00852	1291.	81.
0.0295	0.00882	969.	80.
0.0305	0.00911	1231.	81.
0.0315	0.00941	1114.	82.
0.0325	0.00970	1168.	85.
0.0335	0.00999	1008.	79.
0.0345	0.01029	1117.	81.
0.0355	0.01058	1140.	78.
0.0365	0.01088	1232.	76.
0.0375	0.01117	1020.	76.
0.0385	0.01146	1116.	77.
0.0395	0.01176	1134.	70.
0.0405	0.01205	1198.	77.
0.0415	0.01234	887.	72.
0.0425	0.01263	1297.	74.
0.0435	0.01292	1103.	72.
0.0445	0.01322	1055.	70.
0.0455	0.01351	975.	76.
0.0465	0.01380	1097.	72.
0.0475	0.01409	1125.	72.
0.0485	0.01438	1079.	66.
0.0495	0.01467	1068.	71.
0.0505	0.01496	933.	63.
0.0515	0.01525	1076.	70.
0.0525	0.01554	949.	70.
0.0535	0.01583	989.	64.
0.0545	0.01612	970.	65.
0.0555	0.01641	1165.	67.
0.0565	0.01670	981.	69.
0.0575	0.01699	927.	62.
0.0585	0.01727	968.	63.
0.0595	0.01756	867.	65.
0.0605	0.01785	973.	63.
0.0615	0.01814	752.	58.
0.0625	0.01843	905.	59.
0.0635	0.01871	889.	65.
0.0645	0.01900	844.	62.
0.0655	0.01929	953.	61.

Table 3

The $\bar{p}p$ differential elastic cross-sections at 757 MeV/c. The quoted errors are statistical only. In column 4 are listed the corrections applied to the data for the small-angle trigger acceptance (t.c.), and in column 5 the corrections for the particle absorption in the material of the carbon target only (a.c.).

θ^2 (rad^2)	$-t$ (GeV/c)^2	$d\sigma_m/dt$ [mb/(GeV/c)^2]	t.c.	a.c.
0.0006	0.00038	46215. ± 510.	2.09	1.221
0.0010	0.00064	5627. 136.	1.51	1.248
0.0014	0.00090	2723. 85.	1.25	1.239
0.0020	0.00128	1468. 40.	1.08	1.172
0.0028	0.00179	1120. 33.	1.02	1.085
0.0036	0.00230	977. 29.	1.01	0.994
0.0045	0.00287	938. 33.	1.00	0.976
0.0055	0.00351	908. 33.	1.00	0.963
0.0065	0.00415	890. 31.	1.00	0.977
0.0075	0.00478	892. 30.	1.00	0.992
0.0085	0.00542	811. 28.	1.00	0.981
0.0095	0.00605	860. 29.	1.00	0.995
0.0105	0.00669	809. 29.	1.00	1.000
0.0115	0.00732	857. 28.	1.00	1.000
0.0125	0.00795	815. 28.	1.00	1.000
0.0135	0.00858	767. 28.	1.00	1.000
0.0145	0.00921	754. 26.	1.00	1.000
0.0155	0.00984	740. 25.	1.00	1.000
0.0165	0.01047	739. 26.	1.00	1.000
0.0175	0.01110	770. 27.	1.00	1.000
0.0185	0.01173	728. 26.	1.00	1.000
0.0195	0.01236	810. 26.	1.00	1.000
0.0205	0.01299	713. 26.	1.00	1.000
0.0215	0.01362	755. 25.	1.00	1.000
0.0225	0.01424	719. 24.	1.00	1.000
0.0235	0.01487	701. 25.	1.00	1.000
0.0245	0.01549	732. 25.	1.00	1.000
0.0255	0.01612	667. 24.	1.00	1.000
0.0265	0.01674	687. 23.	1.00	1.000
0.0275	0.01736	642. 23.	1.00	1.000
0.0285	0.01799	621. 23.	1.00	1.000
0.0295	0.01861	692. 24.	1.00	1.000
0.0305	0.01923	672. 23.	1.00	1.000
0.0315	0.01985	638. 22.	1.00	1.000
0.0325	0.02047	633. 24.	1.00	1.000
0.0335	0.02109	614. 22.	1.00	1.000
0.0345	0.02171	647. 23.	1.00	1.000
0.0355	0.02233	625. 22.	1.00	1.000
0.0365	0.02295	604. 22.	1.00	1.000
0.0375	0.02356	587. 22.	1.00	1.000
0.0385	0.02418	561. 21.	1.00	1.000
0.0395	0.02480	616. 22.	1.00	1.000
0.0405	0.02541	573. 21.	1.00	1.000
0.0415	0.02603	601. 21.	1.00	1.000
0.0425	0.02664	594. 21.	1.00	1.000
0.0435	0.02726	528. 21.	1.00	1.000
0.0445	0.02787	576. 21.	1.00	1.000
0.0455	0.02848	549. 21.	1.00	1.000
0.0465	0.02909	530. 20.	1.00	1.000
0.0475	0.02970	527. 20.	1.00	1.000
0.0485	0.03031	492. 19.	1.00	1.000
0.0495	0.03092	569. 21.	1.00	1.000
0.0505	0.03153	544. 20.	1.00	1.000
0.0515	0.03214	522. 20.	1.00	1.000
0.0525	0.03275	514. 20.	1.00	1.000
0.0535	0.03336	508. 20.	1.00	1.000
0.0545	0.03397	494. 20.	1.00	1.000
0.0555	0.03457	509. 20.	1.00	1.000
0.0565	0.03518	514. 20.	1.00	1.000
0.0575	0.03578	479. 19.	1.00	1.000
0.0585	0.03639	477. 19.	1.00	1.000
0.0595	0.03699	490. 19.	1.00	1.000
0.0605	0.03760	490. 19.	1.00	1.000
0.0615	0.03820	468. 19.	1.00	1.000
0.0625	0.03880	466. 19.	1.00	1.000
0.0635	0.03940	419. 18.	1.00	1.000
0.0645	0.04000	441. 18.	1.00	1.000
0.0655	0.04060	434. 18.	1.00	1.000
0.0665	0.04120	410. 18.	1.00	1.000
0.0675	0.04180	395. 18.	1.00	1.000
0.0685	0.04240	438. 19.	1.00	1.000
0.0695	0.04300	409. 18.	1.00	1.000

Table 4

The $\bar{p}p$ differential elastic cross-sections at 1077 MeV/c. The quoted errors are statistical only. In column 4 are listed the corrections applied to the data for the small-angle trigger acceptance (t.c.), and in column 5 the corrections for the particle absorption in the material of the carbon target only (a.c.).

θ^2 (rad^2)	$-t$ (GeV/c)^2	$d\sigma_m/dt$ [mb/(GeV/c)^2]		t.c.	a.c.
0.0005	0.00060	2853.	± 74.	2.04	1.134
0.0007	0.00085	1427.	48.	1.68	1.145
0.0012	0.00145	917.	17.	1.27	1.169
0.0020	0.00242	675.	13.	1.07	1.128
0.0028	0.00338	635.	12.	1.03	1.042
0.0036	0.00435	605.	12.	1.01	0.997
0.0045	0.00543	560.	13.	1.00	0.984
0.0055	0.00663	603.	13.	1.00	0.972
0.0065	0.00783	570.	12.	1.00	0.996
0.0075	0.00903	562.	12.	1.00	1.000
0.0085	0.01023	578.	12.	1.00	1.000
0.0095	0.01143	555.	12.	1.00	1.000
0.0105	0.01262	556.	11.	1.00	1.000
0.0115	0.01382	506.	11.	1.00	1.000
0.0125	0.01501	516.	11.	1.00	1.000
0.0135	0.01620	499.	11.	1.00	1.000
0.0145	0.01739	506.	11.	1.00	1.000
0.0155	0.01858	488.	11.	1.00	1.000
0.0165	0.01977	461.	10.	1.00	1.000
0.0175	0.02095	452.	10.	1.00	1.000
0.0185	0.02214	457.	10.	1.00	1.000
0.0195	0.02332	460.	10.	1.00	1.000
0.0205	0.02450	445.	10.	1.00	1.000
0.0215	0.02568	441.	10.	1.00	1.000
0.0225	0.02686	430.	9.	1.00	1.000
0.0235	0.02804	442.	9.	1.00	1.000
0.0245	0.02921	404.	9.	1.00	1.000
0.0255	0.03039	401.	9.	1.00	1.000
0.0265	0.03156	411.	9.	1.00	1.000
0.0275	0.03273	399.	9.	1.00	1.000
0.0285	0.03390	393.	9.	1.00	1.000
0.0295	0.03507	365.	9.	1.00	1.000
0.0305	0.03624	370.	9.	1.00	1.000
0.0315	0.03740	376.	9.	1.00	1.000
0.0325	0.03857	358.	8.	1.00	1.000
0.0335	0.03973	365.	9.	1.00	1.000
0.0345	0.04089	356.	8.	1.00	1.000
0.0355	0.04205	347.	8.	1.00	1.000
0.0365	0.04321	327.	8.	1.00	1.000
0.0375	0.04437	330.	8.	1.00	1.000
0.0385	0.04552	321.	8.	1.00	1.000
0.0395	0.04668	324.	8.	1.00	1.000
0.0405	0.04783	318.	8.	1.00	1.000
0.0415	0.04898	299.	8.	1.00	1.000
0.0425	0.05013	300.	8.	1.00	1.000
0.0435	0.05128	288.	8.	1.00	1.000
0.0445	0.05243	290.	8.	1.00	1.000
0.0455	0.05358	281.	8.	1.00	1.000
0.0465	0.05472	277.	7.	1.00	1.000
0.0475	0.05586	265.	7.	1.00	1.000
0.0485	0.05701	267.	7.	1.00	1.000
0.0495	0.05815	255.	7.	1.00	1.000
0.0505	0.05929	269.	7.	1.00	1.000
0.0515	0.06043	249.	7.	1.00	1.000
0.0525	0.06156	251.	7.	1.00	1.000
0.0535	0.06270	240.	7.	1.00	1.000
0.0545	0.06383	232.	7.	1.00	1.000
0.0555	0.06496	238.	7.	1.00	1.000
0.0565	0.06610	222.	7.	1.00	1.000
0.0575	0.06723	223.	7.	1.00	1.000
0.0585	0.06835	211.	7.	1.00	1.000
0.0595	0.06948	209.	7.	1.00	1.000
0.0605	0.07061	200.	6.	1.00	1.000
0.0615	0.07173	205.	7.	1.00	1.000
0.0625	0.07286	201.	7.	1.00	1.000
0.0635	0.07398	200.	7.	1.00	1.000
0.0645	0.07510	199.	6.	1.00	1.000
0.0655	0.07622	204.	6.	1.00	1.000
0.0665	0.07734	178.	6.	1.00	1.000
0.0675	0.07845	182.	6.	1.00	1.000
0.0685	0.07957	178.	6.	1.00	1.000
0.0695	0.08068	186.	6.	1.00	1.000

Table 5

Results of the fits at the three momenta: ϱ is the real-to-imaginary ratio, b the nuclear slope, σ_{tot} the $\bar{p}p$ total cross-section, and ν the number of degrees of freedom of the fit; ϱ and b are the results of the fit, whilst σ_{tot} is a fixed parameter. The range of t has been limited in the fit to avoid difficulties in reproducing the steep Coulomb descent, at very small t (at 550 and 757 MeV/c), and to allow a possible t-dependence of the nuclear slope b at large t.

Momentum (MeV/c)	ϱ	b $(GeV/c)^{-2}$	σ_{tot} (mb)	ν	χ^2/ν	Range in $-t$ $\times 10^{-3}(GeV/c)^2$
550	0.084 ± 0.049	20.9 ± 2.1	163.5	47	1.7	0.48–14.8
757	0.102 ± 0.035	18.0 ± 0.5	133	65	1.7	0.77–42.1
1077	0.059 ± 0.024	15.2 ± 0.3	112	48	2.8	0.48–57.6

Figure captions

Fig. 1 Schematic view of the apparatus at a) 550 MeV/c and b) 757 and 1077 MeV/c; B0–2, S1–5, P, P1–5, L1–2, and V are scintillation counters; PC1–9 are multiwire proportional chambers.

Fig. 2 The $\bar{p}p$ measured differential elastic cross-section $d\sigma/dt$ (mb/(GeV/c)^2) as a function of t, corrected for the small-angle trigger acceptance and particle absorption, at 550 MeV/c (a), 757 MeV/c (b), and 1077 MeV/c (c); the errors are statistical only. The superimposed curve is the differential elastic cross-section, folded with the experimental resolution, calculated for the value of ϱ and b resulting from the best fit (table 3); the t-range used in the fit is indicated. No spin dependence is assumed ($\eta = 0$).

Fig. 3 A compilation of the results of ϱ measurements from various experiments below 1.2 GeV/c: pre-LEAR data [1–6, 24] (open circles); this experiment (including the low-momentum points [12] (full circles); other LEAR measurements [7, 8] (full triangles).

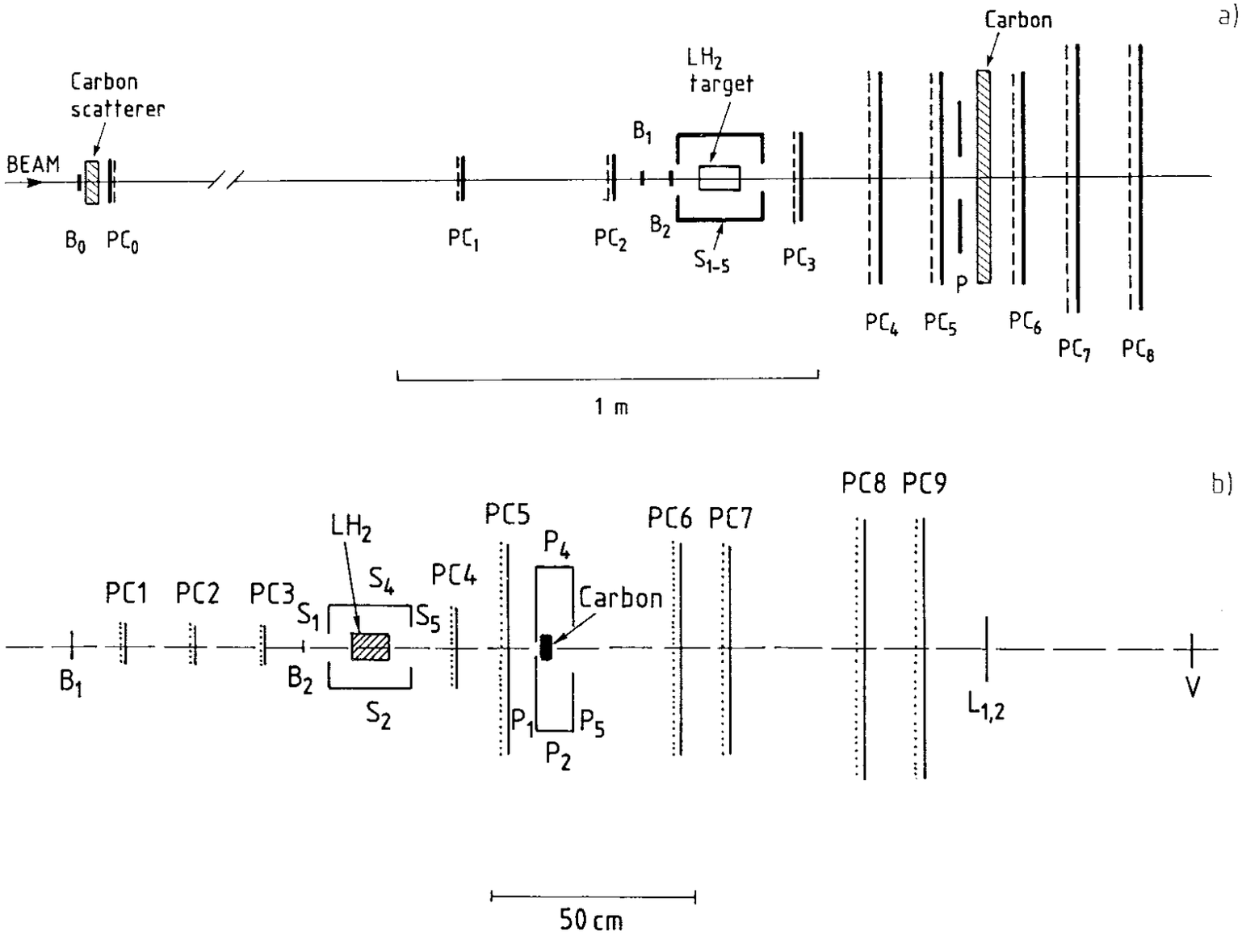
a)
Carbon
scatterer
BEAM
B_0 PC_0
PC_1
PC_2
B_1
LH_2
target
B_2
S_{1-5}
PC_3
Carbon
P
PC_4 PC_5 PC_6 PC_7 PC_8
1 m
b)
PC8 PC9
PC5
PC6 PC7
LH_2
P_4
S_4
PC4
PC1 PC2 PC3
S_1
S_5
Carbon
B_1
B_2
S_2
P_1
P_5
P_2
$L_{1,2}$
V
50 cm

Fig. 1

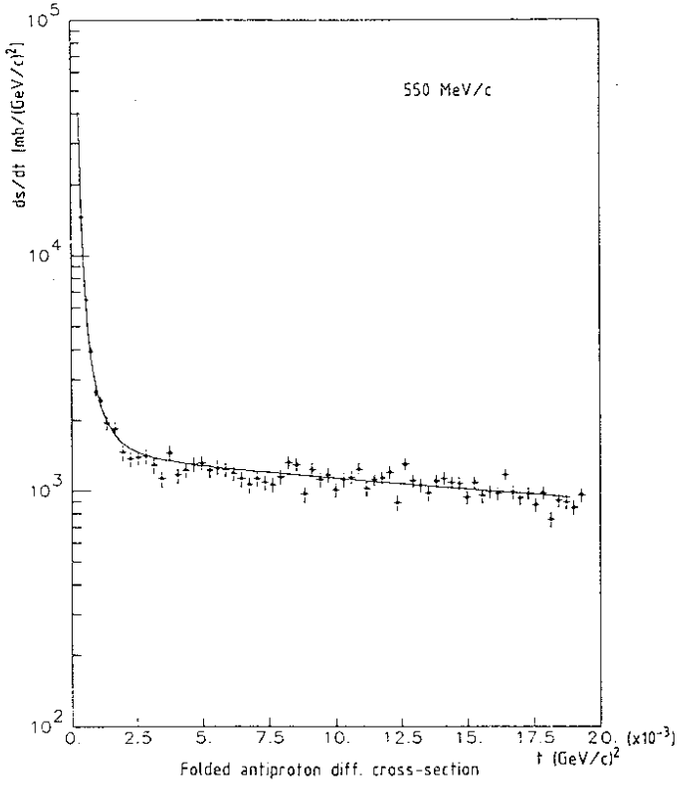
550 MeV/c
ds/dt [mb/(GeV/c)²]
Folded antiproton diff. cross-section
t (GeV/c)²
(x10⁻³)

a)

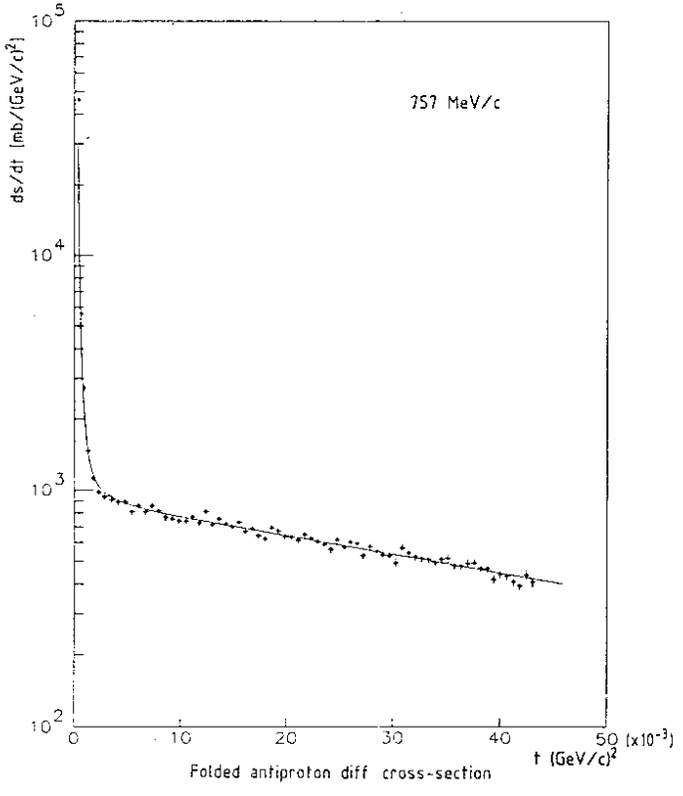
757 MeV/c
ds/dt [mb/(GeV/c)²]
Folded antiproton diff. cross-section
t (GeV/c)²
(x10⁻³)

b)

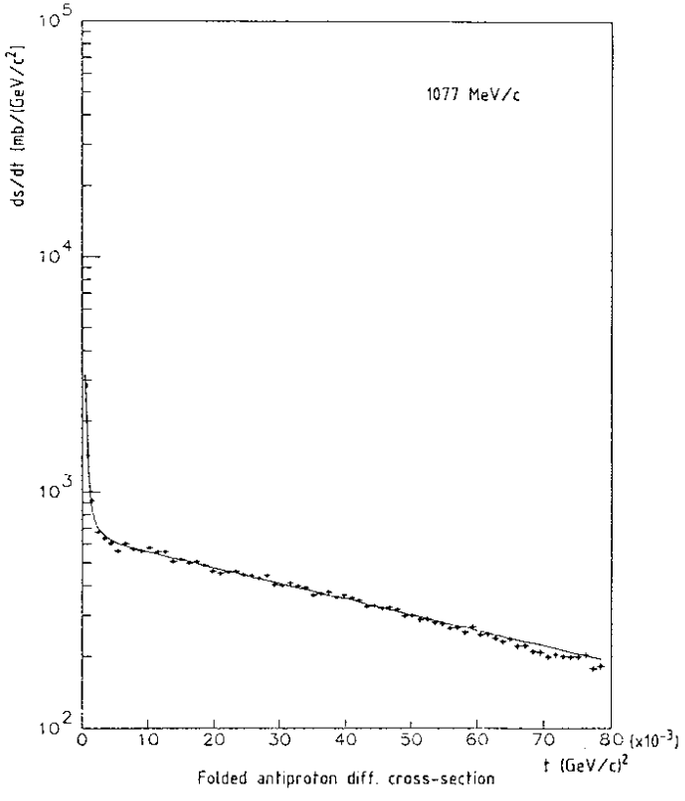
1077 MeV/c
ds/dt [mb/(GeV/c)²]
Folded antiproton diff. cross-section
t (GeV/c)²
(x10⁻³)

c)

Fig. 2

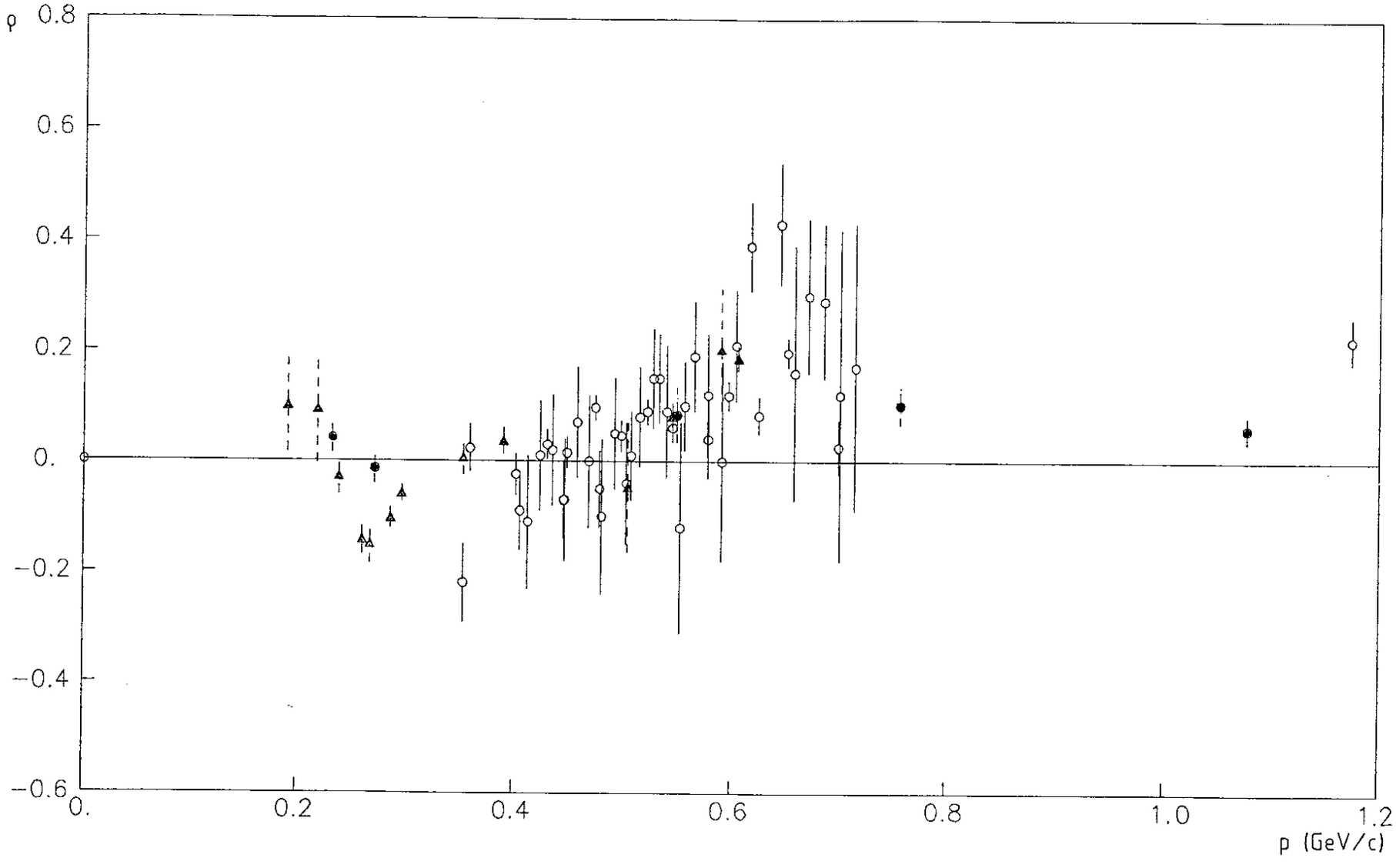

Fig. 3